

# A simple 3D printed microfluidic device for point-of-care analysis of urinary uric acid

Kolsoum Dalvand<sup>A</sup>, Alireza Ghiasvand<sup>A,B,\*</sup> , Sepideh Keshan-Balavandy<sup>B</sup>, Feng Li<sup>B</sup> and Michael Breadmore<sup>B</sup>

For full list of author affiliations and declarations see end of paper

**\*Correspondence to:**

Alireza Ghiasvand  
Department of Chemistry, Lorestan University, Khorramabad, Iran  
Email: [alireza.ghiasvand@utas.edu.au](mailto:alireza.ghiasvand@utas.edu.au)

**Handling Editor:**

John Wade

## ABSTRACT

Point-of-care testing (POCT) technology allows scientists to monitor and diagnose diseases at the patient site, much faster than classical lab-based methods. Herein, a rapid, simple, and sensitive 3D printed microfluidic device integrated with smartphone-based on-chip detection is described for POCT quantification of urinary uric acid. The device includes two circular inputs each connected to a microliter-scale chamber, separated by an integrated porous membrane, located between the sample and reagent chambers. The microfluidic device was fabricated from a transparent photopolymer using a 3D printer, in a single run. The concentration of uric acid was determined based on a chromogenic reaction in which ferrous ion, produced via the reduction of ferric ion by the analyte, complexed with 1,10-phenanthroline, and the color was recorded by a smartphone. Response surface methodology including a central composed design was utilized to evaluate the experimental parameters and subsequent introduction of a multivariate model to describe the experimental conditions. Under the optimum conditions, the calibration curve was linear over the concentration range of 30–600 mg L<sup>-1</sup>. The limit of detection was determined to be 10.5 mg L<sup>-1</sup>. The microfluidic device was successfully utilized for the recovery and quantification of uric acid in the urine, with recoveries ranging from 91.7 to 99.7%.

**Keywords:** 1,10-phenanthroline, 3D printing, colorimetric detection, microfluidic, point-of-care testing, smartphone-based on-chip detection, uric acid, urine.

## Introduction

Uric acid (7,9-dihydro-1H-purine-2,6,8(3H)-trione), composed of welded rings of imidazole and pyrimidine, is the end breakdown product of dietary or endogenous purines.<sup>[1]</sup> Uric acid concentration in urine and blood serum for healthy persons is within the ranges of 250–750 mg L<sup>-1</sup> and 15–80, respectively. Diseases such as leukemia, hyperuricemia, Lesch–Nyhan syndrome, gout, lymphoma, and renal failure cause high levels of serum uric acid (SUA) and consequently high levels of uric acid in the urine.<sup>[2]</sup> Moreover, high uric acid levels can be associated with diabetes and high cholesterol.<sup>[3]</sup> Accordingly, monitoring uric acid levels in blood and urine is a very useful marker for disease diagnosis. Various analytical methods have been reported for the measurement of uric acid in human urine and blood, which can be classified into enzymatic and non-enzymatic methods. Uricase catalysts fit in the enzymatic methods and generate carbon dioxide, allantoin, and hydrogen peroxide from uric acid. Uric acid concentration is then determined by measuring hydrogen peroxide.<sup>[4]</sup> In the non-enzymatic procedure, uric acid is determined directly, for example using electrophoresis,<sup>[5]</sup> liquid chromatography,<sup>[6]</sup> spectrofluorimetry,<sup>[7]</sup> or electrochemical methods.<sup>[8]</sup> Although these procedures have acceptable sensitivity and selectivity for the measurement of uric acid, they are lab-based techniques, time-consuming, and generally need large sample volumes and expensive instrumentations. To address this challenge, many efforts have been dedicated to developing simple and low-cost portable devices for point-of-care testing of clinical markers, like uric acid.<sup>[9]</sup> Micro total analysis systems or lab-on-a-chip systems have been introduced in recent years to reduce analysis time, labor, and cost of chemical

Received: 14 August 2022

Accepted: 8 December 2022

Published: 10 February 2023

**Cite this:**

Dalvand K et al. (2023)  
*Australian Journal of Chemistry*  
76(2), 74–80. doi:[10.1071/CH22180](https://doi.org/10.1071/CH22180)

© 2023 The Author(s) (or their employer(s)). Published by CSIRO Publishing.

This is an open access article distributed under the Creative Commons Attribution-NonCommercial-NoDerivatives 4.0 International License ([CC BY-NC-ND](https://creativecommons.org/licenses/by-nc-nd/4.0/))

OPEN ACCESS

analysis of biological, clinical, and environmental samples, particularly based on microfluidic chips.<sup>[10–12]</sup> Microfluidic technologies have well proven their reliability and applicability for the preparation of point-of-care testing (POCT) devices for disease screening and on-site diagnosis, due to their useful features of high throughput, high speed, low-cost, low sample consumption, and simplicity.<sup>[13]</sup>

So far, different microfluidic systems have been used for diagnosis and monitoring diseases such as diabetes, cardiovascular disease, renal disease, and cancer.<sup>[14]</sup> Rossini *et al.* employed a paper-based microfluidic analytical device for the simultaneous quantification of uric acid and creatinine in urine.<sup>[15]</sup> Chen *et al.* used a 3D-printed paper-based microfluidic device and used it for bienzyme colorimetric determination of uric acid and glucose in human serum.<sup>[16]</sup> However, traditional technologies to produce microfluidic devices such as soft lithography, laser ablation, micro-machining, hot embossing, and injection molding are expensive, require skilled operators, and sophisticated instruments. They have also limited options for the preparation of biocompatible systems.<sup>[17,18]</sup>

3D printing technology is a promising alternative to address these limitations and can be used for low-cost and fast fabrication of micro/mesofluidic devices with complex geometry with high repeatability.<sup>[19]</sup> Among different commercially available 3D printing technologies, PolyJet is preferred for the fabrication of small objects with more details and fine surface finishing like microfluidic devices that need higher structural resolution.<sup>[20]</sup> In PolyJet printing, liquid photopolymers are jetted through linearly arranged nozzles and the resultant microdroplets sprayed onto the build surface, where the materials are solidified by being irradiated using ultraviolet light. These printers have a high throughput but offer a limited selection of photopolymer build materials.<sup>[21]</sup>

This research reports and evaluates a low-cost and simple microfluidic device for POCT quantification of uric acid in urine. The 3D printed microfluidic device was fabricated by a transparent photopolymer by a PolyJet printer in a single run and employed for indirect image-based colorimetric determination of uric acid using a smartphone. The influential parameters on the performance of the smartphone-based microfluidic system were optimized via a response surface methodology (RSM) including central composite design (CCD).

## Experimental section

### Chemicals and apparatus

Analytical reagent grade uric acid, 1,10-phenanthroline, Fe (NO<sub>3</sub>)<sub>3</sub>.9H<sub>2</sub>O and all other acids, bases, and salts were purchased from Merck (Darmstadt, Germany). A standard stock solution (1000 µg mL<sup>-1</sup>) of uric acid was prepared in 0.05 mol L<sup>-1</sup> sodium hydroxide solution. The working

standard solutions were made by diluting the corresponding stock solution with 0.01 M phosphate-buffered saline solution (pH ~7.4). PolyJet water-soluble support material (SUP7070) and build material (VeroClear™ RGD810, transparent photopolymer) were provided by Stratasys (Eden Prairie, MN, USA). An Objet Eden260VS 3D printer from Stratasys was used for 3D printing of the chips with a resolution of 600 × 600 × 1600 dpi and a 16-µm layer thickness. An Orbital Shaker SO1 from Stuart Scientific (Staffordshire, UK) was utilized to remove the support material from the chips by washing with 0.2% NaOH solution. A Shimadzu UV-1650 PC spectrophotometer was used to record absorption spectra of uric acid and Fe<sup>2+</sup>/1,10-orthophenanthroline complex.

### Design and fabrication of microfluidic chip

The microfluidic device with an integrated membrane between the chambers was printed using the PolyJet printer in a single run as described previously.<sup>[21]</sup> Briefly, the chip was first designed by Version 2016 AutoCAD software (Autodesk Inc., CA, USA). The CAD files were then transformed to STL format and sliced into G-codes (ready to print) by KISSlicer PRO software. The chip contains two 35-µL chambers interconnected by a porous membrane. Each chamber has a circular hole as input. The sample chamber was designed in a rectangular shape, with a triangular channel reagent chamber.

The dimensions of the microfluidic device were 40 × 20 × 1.4 mm. After printing, surplus layers of the support were first removed using a knife, and the chips were rinsed several times with 0.2% NaOH solution. Then, they were soaked in 0.2% NaOH solution and shaken for 24 h, for the complete removal of the support material and cleaning of the chambers. Finally, the microfluidic devices were dried at ambient temperature on a clean aluminum foil and kept in sealed plastic bags. To avoid the adsorption of analytes onto chambers and the membrane, each microfluidic device was used in a single test.

## Results and discussion

### Smartphone-based colorimetric microfluidic determination of uric acid

Uric acid is a strong electron donor (reducing agent), and this characteristic was exploited to develop a strategy for its determination via a smartphone-based colorimetric microfluidic method.<sup>[22]</sup> For this purpose, first, ferric ion (Fe<sup>3+</sup>) was reduced by uric acid and converted to ferrous ion (Fe<sup>2+</sup>). Then, ferrous ion was reacted with 1,10-phenanthroline to form ferroin (a 1:3 complex, [Fe(phen)<sub>3</sub>]<sup>2+</sup>) and immediately generated a pale-yellow color in the pH range 2–9. Ferroin is a suitable redox

indicator and is widely applied in titrimetry, particularly cerimetric titration. Its color change is reversible and very fast. The color of Ferroin solutions is stable for several weeks at temperatures up to 60°C. The overall reaction of  $\text{Fe}^{3+}$  with uric acid in the presence of 1,10-phenanthroline is depicted in Fig. 1.

For colorimetric determination of uric acid using the microfluidic device, 35  $\mu\text{L}$  uric acid solution (sample) was injected into the rectangular chamber and then 35  $\mu\text{L}$  of chromogenic reagent ( $\text{Fe}^{3+}$ -1,10-phenanthroline) mixture was injected into the triangular chamber and left to equilibrate (room temperature, 12.5 min).

Fig. 2 shows the images of a microfluidic device before and after the injection of the chromogenic reagent and sample. The sample chamber was colorless at first but turned pale yellow as the chromogenic reagent began to penetrate the sample. After completing color development, the sample chamber turned red. Then, a smartphone was used to photograph the microfluidic devices at a distance of 10 cm. The processing of the obtained images was accomplished using Image J (<https://imagej.nih.gov/ij>). The recorded intensities were transformed to greyscale after subtracting the intensity of the background. Then the responses of the samples were compared to a standard calibration graph. The design that illustrates the whole set operating protocol for the smartphone-based colorimetric determination of urinary uric acid is shown in

Supplementary Fig. S1 and the injection, color development, and data processing steps are depicted in Supplementary Fig. S2.

### Optimization of the smartphone-based colorimetric method using RSM-CCD

RSM uses a low-order polynomial equation in a predefined range of a set of independent variables. It is then analyzed to determine the optimal values of the variables in order to obtain the best response.<sup>[23]</sup> Multivariate optimization is faster than a one-at-a-time strategy and requires fewer experimental runs. It is also able to clarify the interactions between the factors. Therefore, response surface methodology was used to identify the parameters that had the greatest influence on the chromogenic reaction, including reaction time, the concentration of ferric ion, and concentration of 1,10-phenanthroline. CCD, as a response surface strategy, combines a two-level factorial design with a star design and center points.<sup>[24]</sup> The number of experimental runs ( $N$ ) for a CCD with  $k$  factors and  $C_p$  center points is defined by:

$$N = k^2 + 2k + C_p \quad (1)$$

Three factors were defined as reaction time (min), concentrations of 1,10-phenanthroline ( $\text{mol L}^{-1}$ ), and concentrations

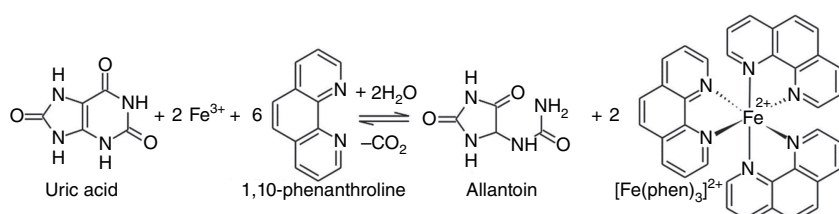


**Fig. 1.** The reaction of uric acid with ferric ion in the presence of 1,10-phenanthroline and formation of ferroin.

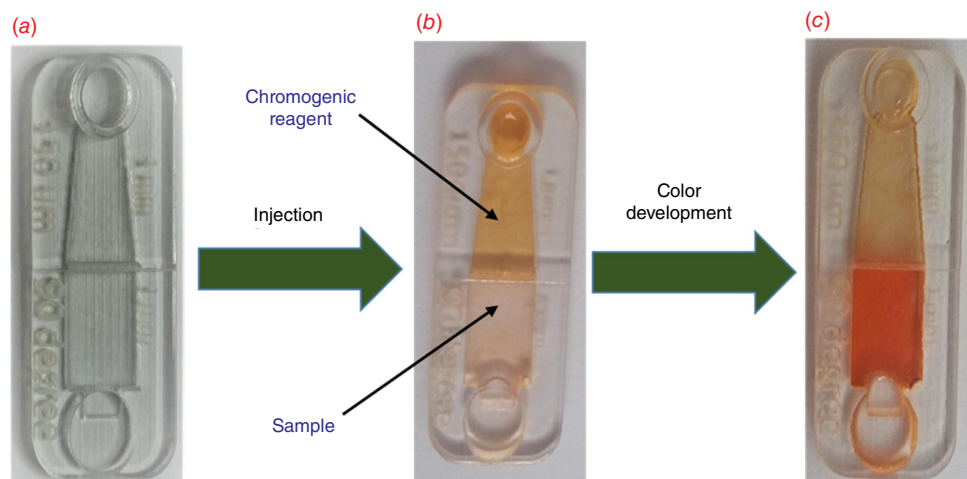


**Fig. 2.** The microfluidic device before injection (a), after injection of sample and chromogenic reagent (b), and after complete color development (c).

of  $\text{Fe}^{3+}$  ( $\text{mol L}^{-1}$ ), at five center points (Supplementary Table S1). This means that 20 test runs had to be performed. The experimental matrix was designed using Minitab 19 statistical software (Minitab Inc., State College, PA, USA). The CCD experimental matrix and the obtained responses are given in Supplementary Table S2. Color intensity, recorded by the smartphone, was selected as the response.

A second-order polynomial equation has resulted from the multiple linear regression (Eqn 2). It explains the relationship between color intensity and the experimental factors as:

$$\begin{aligned} \text{Intensity} = & -92.07 + 10.086A + 1517.9B \\ & + 1879.6C - 0.350A^2 - 6243B^2 \\ & - 18842C^2 - 31.48AB + 20.12AC \\ & - 2616BC \end{aligned} \quad (2)$$

A two-way ANOVA was employed to compare the differences in the responses. The ANOVA was performed using Fisher statistical analysis and the results are shown in Supplementary Table S3. Based on the results, all studied variables had significant effects on the response ( $P < 0.05$ ). A  $P$ -value of less than 0.05 indicates a parameter that is statistically significant, at 95% confidence level. The 'Lack of Fit' for the  $F$ -value is 0.682, which demonstrates it isn't

significant relative to the pure error, confirming the validity of the second-order polynomial model. Furthermore, the high coefficient of determination  $R^2$  (99.83%), adjusted  $R^2$  (99.61%), and predicted  $R^2$  (99.32%) show an acceptable correlation between the experimental variables and the selected model.<sup>[25]</sup> In addition, the response surface plots (Fig. 3a) were used to optimize the variables and evaluate the interactive effects of the independent factors, while the other factors were kept constant at their optimal values. As the results show, the optimum values of reaction time, the concentration of  $\text{Fe}^{3+}$ , and the concentration of 1,10-phenanthroline were predicted 12.5 (min), 0.05 ( $\text{mol L}^{-1}$ ), and 0.08 ( $\text{mol L}^{-1}$ ), respectively. Fig. 3a also shows that the color intensity increases with reaction time to 12.5 min and then decreases. On the other hand, raising of  $\text{Fe}^{3+}$  and phenanthroline concentrations leads to an increase in color intensity with reaction time. The contour plots are presented in Fig. 3b, showing that there is no direct linear relationship between the selected independent variables.

The interaction between the parameters is shown in the plot interaction diagram (Supplementary Fig. S3). Non-parallel lines indicate the interaction between parameters. The diagram shows there are interactions between Time/ $C_{\text{phen}}$  and Time/ $C_{\text{Fe}^{3+}}$ , but there is no interaction between  $C_{\text{phen}}/C_{\text{Fe}^{3+}}$ .

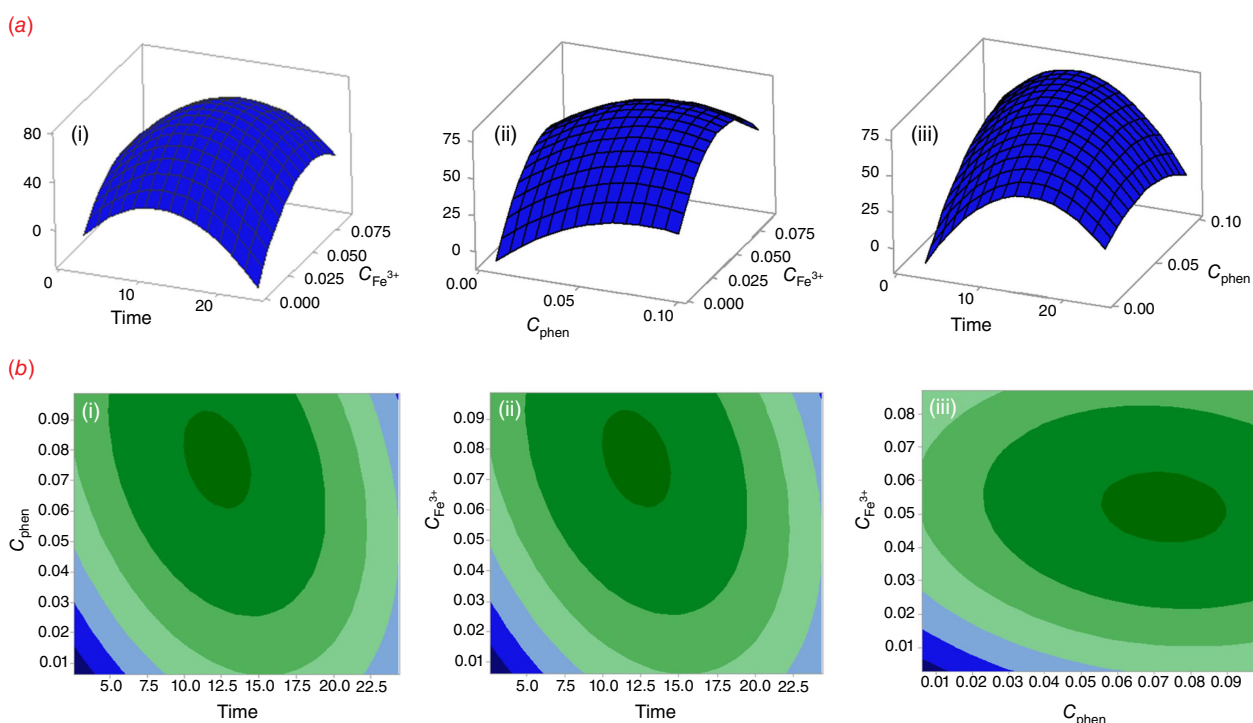


**Fig. 3.** (a) Response surfaces obtained from the central composite design, (i)  $\text{Fe}^{3+}$  concentration vs reaction time, (ii) reaction time vs phenanthroline concentration, and (iii)  $\text{Fe}^{3+}$  concentration vs phenanthroline concentration. (b) Contour plots obtained from the central composite design for phenanthroline concentration and reaction time (i),  $\text{Fe}^{3+}$  concentration and reaction time (ii), and  $\text{Fe}^{3+}$  concentration and phenanthroline concentration (iii).

## Analytical figures of merit and real sample

The smartphone-based colorimetric method proposed in this research was evaluated by obtaining the analytical figures of merit, including, the limit of detection (LOD), relative standard deviation (RSD), and linear dynamic range (LDR). The calibration graph was linear over the range of 30–600 mg L<sup>-1</sup> ( $R^2 = 0.992$ ). The LOD (three times the blank's standard deviation,  $3\sigma$ ) was 10.5 mg L<sup>-1</sup>. RSD for six replicated analyzes of a sample containing 250 mg L<sup>-1</sup> of uric acid was found to be 7.9%. The calibration graph and color change for different concentrations of uric acid obtained while generating the calibration graph are presented in Supplementary Figs S4 and S5, respectively.

To assess the applicability of the developed method for real samples, it was utilized for the measurement of uric acid in three human urine samples, collected from a local Pathobiology Laboratory (Khorramabad, Iran), in accordance with relevant guidelines and regulations. To ensure the accuracy and reliability of the obtained results, all samples were also fortified with a standard solution at three levels (close to low-quality control (LQC), medium quality control (MQC), and high-quality control (HQC)) according to the International Council for Harmonisation of Technical Requirements for Pharmaceuticals for Human Use recommendations<sup>[11,26]</sup> and subjected to the developed method in triplicate (Table 1). Recoveries were obtained in the range of 91.7–99.7%, demonstrating that the proposed microfluidic device and smartphone-based colorimetric procedure can be successfully applied for the determination of uric acid in urine samples.

For further evaluation of the reliability and validity of the developed method, its analytical performance was compared with similar published studies on the determination of uric acid.<sup>[9,15,16,27]</sup> The results (Table 2) showed that the

**Table 1.** Recovery of uric acid from human urine samples spiked at three levels within the LDR.

Sample	Uric acid concentration (mg L <sup>-1</sup> )		Recovery (%)
	Added	Found	
Urine (1)	0	0.1	—
	100	92.0 (10.9)	92.0
	250	249.9 (8.6)	99.7
	400	390.5 (7.1)	97.9
	0	0.06	—
Urine (2)	100	91.5 (10.1)	91.7
	250	230.5 (7.6)	92.3
	400	379.2 (5.7)	94.6
	0	0.1	—
Urine (3)	100	94.4 (8.4)	94.0
	250	237.9 (6.9)	95.4
	400	385.2 (5.1)	96.2

RSDs in parentheses were calculated based on six replicated experiments.

**Table 2.** Comparison of the smartphone-based microfluidic method with some representative colorimetric procedures for the determination of uric acid.

Technique	Detection strategy	Indicator	Colorimetric device	LOD (mg/L)	RSD (%)	Matrix	Ref.
HPAD <sup>A</sup>	Colorimetric determination with enzymatic bioassays	4-AAPI/DHBS <sup>B</sup>	HP office scanner	6.2	3.6–9	Serum	[9]
HPAD	Gel Documentation	4-AAPI/DHBS	Common camera	42.2	4.97–8.57	Serum	[16]
HPAD	Colorimetry	Fe <sup>3+</sup> /l,10-phenanthroline	Simple digital colorimetry	16.5	5.8–8.3	Urine	[15]
HPAD	Colorimetry	Commercial alanine aminotransferase (ALT) <sup>C</sup> assay kit	Sigma-Aldrich ALT assay kit	21.9	—	Standard aqueous solution	[27]
3DP Microfluidic	Colorimetry	Fe <sup>3+</sup> /l,10-phenanthroline	Smartphone	10.5	7.9	Urine	This study

<sup>A</sup>Microfluidic paper-based analytical devices.

<sup>B</sup>4-Aminoantipyrine and sodium 3,5-dichloro-2-hydroxy-benzenesulfonate.

<sup>C</sup>Alanine aminotransferase.

LOD of the proposed procedure is lower than other reported methods, except for the method that utilized chitosan to improve the analytical response of enzymatic bioassay via gel documentation.<sup>[9]</sup> The RSD is also comparable to the values reported for the listed procedures. These studies used photographic cameras,<sup>[27]</sup> benchtop spectrophotometers,<sup>[15]</sup> and benchtop scanners,<sup>[9]</sup> the former two of which impede the portability and point-of-care use of these systems. The only portable setup used in these studies (**Table 2**) is a Sigma-Aldrich ALT assay kit; however, the widespread use of this method would be limited by the high cost of the measurement kit (each kit sufficient for 100 colorimetric or fluorometric tests costs AU\$668, as of 30 March 2022). In contrast, the procedure presented here uses a simple and low-cost colorimetric setup, integrated into a microfluidic chip, and is suitable for real-time and point-of-care analysis of uric acid.

As can be seen from **Table 2**, μPADs are a serious competitor to other microfluidic devices for the point-of-care determination of uric acid. Obviously, they are mostly cheaper than 3D-printed microfluidic devices.<sup>[28,29]</sup> However, 3D-printed microfluidic devices have some advantages over μPADs that cannot be ignored. 3D-printing produces highly reproducible microfluidic devices, whereas it is almost impossible to create μPADs with the same physicochemical properties due to the complex nature of paper chemistry. On the other hand, the moisture content of paper material changes rapidly in different weather conditions and can seriously affect its capillary characteristics, as the basic mechanism for paper-based microfluidic analysis. Additionally, being rigid materials, they are more robust and efficient than paper-based microfluidic devices (paper is flexible and its shape changes with moisture).

## Interference study

Other natural compounds present in the urine can have adverse effects on the colorimetric determination of uric acid content. To evaluate the applicability of the prosed method to real samples with complex matrix, uric acid was determined in the presence of various possible interfering compounds. The results are presented in **Table 3**, and show that most of the tested species did not interfere with

**Table 3.** Tolerance limits of relevant compounds on the SB-3DP-MF analysis of uric acid solutions with a concentration of  $250 \text{ mg L}^{-1}$  (a relative error of 5% was considered tolerable).

Foreign compound	Tolerated ratio ([diverse compound]/[uric acid])
Ascorbic acid	40
Creatinine	100
Citric acid	110
Glucose	90

the uric acid, even in high concentration levels (up to 110 times). However, ascorbic acid showed an interference effect at a concentration ratio of 40, likely due to its reducing potential. However, such a high concentration is unlikely to occur because the normal range of uric acid and ascorbic acid in urine is 35–72 and  $6\text{--}20 \text{ mg L}^{-1}$ , respectively, which is far from the tested ratio of 40. However, suppose the concentration of ascorbic acid is too high (for any reason) to interfere with uric acid. In that case, it can be easily removed from the urine sample by bubbling air into the sample solution.

## Conclusion

A smartphone-based colorimetric method using a 3D-printed microfluidic device was successfully applied for the quantification of urinary uric acid. The smartphone-based color imaging and data processing provide a simple digital read-out for accurate colorimetric determination without the need for sophisticated spectrophotometric detectors. The central composed design was used to optimize the influential variables to minimize the number of experiments in the optimization process, as well as to reveal the significance of the variable and their interactions. Under the optimized conditions, low LOD, wide LDR, and acceptable recovery and reproducibility were achieved. The results showed that the suggested device and strategy can be utilized as a simple, low-cost, and easy-to-operate alternative for POCT analysis of biomarkers in human urine, to be used for evaluation of renal function and monitor kidney function.

## Supplementary material

Supplementary material is available online.

## References

- [1] Khan MI, Zhang Q, Wang YX, Saud S, Liu WW, Liu SR, et al. Portable electrophoresis titration chip model for sensing of uric acid in urine and blood by moving reaction boundary. *Sensor Actuators B Chem* 2019; 286: 9–15. doi:[10.1016/j.snb.2019.01.098](https://doi.org/10.1016/j.snb.2019.01.098)
- [2] Nakanishi N, Okamoto M, Yoshida H, Matsuo Y, Suzuki K, Tatara K. Serum uric acid and risk for development of hypertension and impaired fasting glucose or type ii diabetes in japanese male office workers. *Eur J Epidemiol* 2003; 18: 523–530. doi:[10.1023/A:1024600905574](https://doi.org/10.1023/A:1024600905574)
- [3] Chen JC, Chung HH, Hsu CT, Tsai DM, Kumar AS, Zen JM. A disposable single-use electrochemical sensor for the detection of uric acid in human whole blood. *Sensor Actuators B Chem* 2005; 110: 364–369. doi:[10.1016/j.snb.2005.02.026](https://doi.org/10.1016/j.snb.2005.02.026)
- [4] Azmi NE, Ramli NI, Abdullah J, Abdul Hamid MA, Sidek H, Abd Rahman S, et al. A simple and sensitive fluorescence based biosensor for the determination of uric acid using  $\text{H}_2\text{O}_2$ -sensitive quantum dots/dual enzymes. *Biosens Bioelectron* 2015; 67: 129–133. doi:[10.1016/j.bios.2014.07.056](https://doi.org/10.1016/j.bios.2014.07.056)
- [5] Pavláček V, Tůma P, Matějčková J, Samcová E. Very fast electrophoretic determination of creatinine and uric acid in human urine

- using a combination of two capillaries with different internal diameters. *Electrophoresis* 2014; 35: 956–961. doi:[10.1002/elps.201300293](https://doi.org/10.1002/elps.201300293)
- [6] Remane D, Grunwald S, Hoeke H, Mueller A, Roeder S, von Bergen M, et al. Validation of a multi-analyte HPLC-DAD method for determination of uric acid, creatinine, homovanillic acid, niacinamide, hippuric acid, indole-3-acetic acid and 2-methylhippuric acid in human urine. *J Chromatogr B* 2015; 998–999: 40–44. doi:[10.1016/j.jchromb.2015.06.021](https://doi.org/10.1016/j.jchromb.2015.06.021)
- [7] Martinez-Pérez D, Ferrer ML, Mateo CR. A reagent less fluorescent sol-gel biosensor for uric acid detection in biological fluids. *Anal Biochem* 2003; 322: 238–242. doi:[10.1016/j.ab.2003.08.018](https://doi.org/10.1016/j.ab.2003.08.018)
- [8] Lakshmi D, Whitcombe MJ, Davis F, Sharma PS, Prasad BB. Electrochemical detection of uric acid in mixed and clinical samples: A review. *Electroanalysis* 2011; 23: 305–320. doi:[10.1002/elan.201000525](https://doi.org/10.1002/elan.201000525)
- [9] Gabriel EFM, Garcia PT, Cardoso TMG, Lopes FM, Martins FT, Coltro WKT. Highly sensitive colorimetric detection of glucose and uric acid in biological fluids using chitosan-modified paper microfluidic devices. *Analyst* 2016; 141: 4749–4756. doi:[10.1039/c6an00430j](https://doi.org/10.1039/c6an00430j)
- [10] Yao Y, Zhang C. A novel screen-printed microfluidic paper-based electrochemical device for detection of glucose and uric acid in urine. *Biomed Microdevices* 2016; 18: 92. doi:[10.1007/s10544-016-0115-6](https://doi.org/10.1007/s10544-016-0115-6)
- [11] Naccarato A, Tassone A, Moretti S, Elliani R, Sprovieri F, Pirrone N, et al. A green approach for organophosphate ester determination in airborne particulate matter: Microwave-assisted extraction using hydroalcoholic mixture coupled with solid-phase microextraction gas chromatography-tandem mass spectrometry. *Talanta* 2018; 189: 657–665. doi:[10.1016/j.talanta.2018.07.077](https://doi.org/10.1016/j.talanta.2018.07.077)
- [12] Sohrabi H, Bolandi N, Hemmati A, Eyvazi S, Ghasemzadeh S, Baradaran B, et al. State-of-the-art cancer biomarker detection by portable (bio) sensing technology: A critical review. *Microchem J* 2022; 177: 107248. doi:[10.1016/j.microc.2022.107248](https://doi.org/10.1016/j.microc.2022.107248)
- [13] Tseng C-C, Yang R-J, Ju W-J, Fu L-M. Microfluidic paper-based platform for whole blood creatinine detection. *Chem Eng J* 2018; 348: 117–124. doi:[10.1016/j.cej.2018.04.191](https://doi.org/10.1016/j.cej.2018.04.191)
- [14] Fu L-M, Tseng C-C, Ju W-J, Yang R-J. Rapid paper-based system for human serum creatinine detection. *Inventions* 2018; 3: 34. doi:[10.3390/inventions3020034](https://doi.org/10.3390/inventions3020034)
- [15] Rossini EL, Milani MI, Carrilho E, Pezza L, Pezza HR. Simultaneous determination of renal function biomarkers in urine using a validated paper-based microfluidic analytical device. *Anal Chim Acta* 2018; 997: 16–23. doi:[10.1016/j.aca.2017.10.018](https://doi.org/10.1016/j.aca.2017.10.018)
- [16] Chen X, Chen J, Wang F, Xiang X, Luo M, Ji X, et al. Determination of glucose and uric acid with bienzyme colorimetry on microfluidic paper-based analysis devices. *Biosens Bioelectron* 2012; 35: 363–368. doi:[10.1016/j.bios.2012.03.018](https://doi.org/10.1016/j.bios.2012.03.018)
- [17] Waheed S, Cabot JM, Macdonald NP, Lewis T, Guijt RM, Paull B, et al. 3D printed microfluidic devices: Enablers and barriers. *Lab Chip* 2016; 16: 1993–2013. doi:[10.1039/c6lc00284f](https://doi.org/10.1039/c6lc00284f)
- [18] de Jong J, Lammertink RGH, Wessling M. Membranes and microfluidics: A review. *Lab Chip* 2006; 6: 1125–1139. doi:[10.1039/b603275c](https://doi.org/10.1039/b603275c)
- [19] Calderilla C, Maya F, Cerdà V, Leal LO. 3D printed device including disk-based solid-phase extraction for the automated speciation of iron using the multisyringe flow injection analysis technique. *Talanta* 2017; 175: 463–469. doi:[10.1016/j.talanta.2017.07.028](https://doi.org/10.1016/j.talanta.2017.07.028)
- [20] Keshan Balavandy S, Li F, Macdonald NP, Maya F, Townsend AT, Frederick K, et al. Scalable 3D printing method for the manufacture of single-material fluidic devices with integrated filter for point of collection colourimetric analysis. *Anal Chim Acta* 2021; 1151: 238101. doi:[10.1016/j.aca.2020.11.033](https://doi.org/10.1016/j.aca.2020.11.033)
- [21] Dalvand K, Balavandy SK, Li F, Breadmore M, Ghiasvand A. Optimization of smartphone-based on-site-capable uranium analysis in water using a 3D printed microdevice. *Anal Bioanal Chem* 2021; 413: 3243–3251. doi:[10.1007/s00216-021-03260-4](https://doi.org/10.1007/s00216-021-03260-4)
- [22] Heo SH, Lee S-H. High levels of serum uric acid are associated with silent brain infarction. *J Neurol Sci* 2010; 297: 6–10. doi:[10.1016/j.jns.2010.07.007](https://doi.org/10.1016/j.jns.2010.07.007)
- [23] Bezerra MA, Santelli RE, Oliveira EP, Villar LS, Escaleira LA. Response surface methodology (RSM) as a tool for optimization in analytical chemistry. *Talanta* 2008; 76: 965–977. doi:[10.1016/j.talanta.2008.05.019](https://doi.org/10.1016/j.talanta.2008.05.019)
- [24] Narendran ST, Meyyanathan SN, Karri VVSR. Experimental design in pesticide extraction methods: A review. *Food Chem* 2019; 289: 384–395. doi:[10.1016/j.foodchem.2019.03.045](https://doi.org/10.1016/j.foodchem.2019.03.045)
- [25] Ahmadi M, Vahabzadeh F, Bonakdarpour B, Mofarrah E, Mehranian M. Application of the central composite design and response surface methodology to the advanced treatment of olive oil processing wastewater using fenton's peroxidation. *J Hazard Mater* 2005; 123: 187–195. doi:[10.1016/j.jhazmat.2005.03.042](https://doi.org/10.1016/j.jhazmat.2005.03.042)
- [26] Akram M, Asghar MN, Saleem Khan M, Shahid S, Abdur Rahman HM, Nadeem I. Development and validation of an economical uric acid- $\text{Fe}^{3+}/\text{Fe}^{2+}$ -ferrozine-based colorimetric assay to estimate uric acid level of pure and biological samples. *Biosci Biotechnol Biochem* 2020; 84: 1967–1974. doi:[10.1080/09168451.2020.1781593](https://doi.org/10.1080/09168451.2020.1781593)
- [27] Demirel G, Babur E. Vapor-phase deposition of polymers as a simple and versatile technique to generate paper-based microfluidic platforms for bioassay applications. *Analyst* 2014; 139: 2326–2331. doi:[10.1039/c4an00022f](https://doi.org/10.1039/c4an00022f)
- [28] Vidal E, Lorenzetti AS, Lista AG, Domini CE. Micropaper-based analytical device ( $\mu$ PAD) for the simultaneous determination of nitrite and fluoride using a smartphone. *Microchem J* 2018; 143: 467–473. doi:[10.1016/j.microc.2018.08.042](https://doi.org/10.1016/j.microc.2018.08.042)
- [29] Tsagkaris AS, Migliorelli D, Uttil L, Filippini D, Pulkarbova J, Hajslava J. A microfluidic paper-based analytical device ( $\mu$ PAD) with smartphone readout for chlorpyrifos-oxon screening in human serum. *Talanta* 2021; 222: 121535. doi:[10.1016/j.talanta.2020.121535](https://doi.org/10.1016/j.talanta.2020.121535)

**Data availability.** The data that support this study are available in the article and accompanying online supplementary material.

**Conflicts of interest.** The authors declare no conflicts of interest.

**Declaration of funding.** The authors received no financial support for the research, authorship, and/or publication of this article.

#### Author affiliations

<sup>A</sup>Department of Chemistry, Lorestan University, Khoramabad, Iran.

<sup>B</sup>Australian Centre for Research on Separation Science (ACROSS), School of Natural Sciences, University of Tasmania, Hobart, Tas. 7001, Australia.